Estimation of the contribution of intercontinental transport during the PEACE campaign by using a global model

Masayuki Takigawa,[1] Kengo Sudo,[1] Hajime Akimoto,[1] Kazuyuki Kita,[2] Nobuyuki Takegawa,[3] Yutaka Kondo,[3] and Masaaki Takahashi[1,4]

[1] A quasi−real−time calculation system for the global distribution of ozone (O_3) and its precursors, including CO, NO_x, and nonmethane hydrocarbons (NMHCs), has been newly developed by using a 3−D chemical−transport model. The model is driven by meteorological data from the National Centers for Environmental Prediction (NCEP), and produces daily 7−day forecast of the distribution of chemical species. The model was used in daily flight planning for the Pacific Exploration of Asian Continental Emission (PEACE)−A and −B aircraft measurement campaigns in January and April−May 2002, respectively. Model−calculated meteorological fields show good agreement with aircraft observations. The model also reproduced events such as polluted air masses in the lower troposphere (LT) corresponding to post−frontal outflow, a high−concentration CO plume in the upper troposphere (UT) in late spring, and the observed plume that was transported by deep convection over central China. The amount of CO transported into the free troposphere (FT) by deep convection was estimated to be about 6 Tg CO over China in May 2002. Meridional and seasonal variations in the long−range transport (LRT) of CO tracers, Asian CO tracers, and CO tracers produced from the oxidation of CH_4 and NMHCs were all evaluated using tagged CO tracers. LRT CO comprised about 36% of the total CO budget in December−February 2001/2002, and about 20% in March−May 2002 in the free troposphere over Japan. In late spring, the concentration of Asian CO over southern Japan decreased compared to that in winter because the wind direction shifted from northwesterly to easterly or southerly.

1. Introduction

[2] Field campaigns are essential for a complete understanding of the physical and chemical processes that control trace gases and aerosol concentrations in the atmosphere. Variability in meteorological fields and in chemical processes both alters the distributions of trace gases and aerosols. Therefore, careful planning is required to maximize the use of available resources and meet campaign objectives. Flight planning for field campaigns has traditionally relied on meteorological forecasts and trajectory models. Recently, chemical transport models (CTMs) have

enhanced flight planning by providing direct information on the expected state of important three−dimensional atmospheric chemical structures on timescales of hours to days, i.e., the "chemical weather". The first chemical weather forecasting was during ASHORE (Airborne Southern Hemisphere Ozone Experiment) and SESAME (Second European Stratospheric Arctic and Middle-Latitude Experiment) in 1994 and 1995 [*Lee et al.*, 1997]. *Lee et al.* [1997] used global stratospheric CTMs. The use of chemical weather forecasts for field campaigns is expanding rapidly. Global chemical weather forecasts from MATCH−MPIC (Model of Atmospheric Transport and Chemistry − Max−Planck−Institute for Chemistry version) were used during INDOEX (Indian Ocean Experiment) in 1999 and MINOS (the Mediterranean Intensive Oxidants Study) and CONTRACE (Convective Transport of Trace Gases into the Upper Troposphere over Europe) in 2001 [*Lawrence et al.*, 2003]. In contrast to regional chemical weather forecasts, global chemical weather forecasts can predict intercontinental transport. For example, *Lawrence et al.* [2003] estimated the frequency of intercontinental pollution plumes from North America and Asia to Europe. A global aerosol forecast from the Georgia Tech/Goddard Global Ozone

[1]Frontier Research Center for Global Change, Japan Marine Science and Technology Center, Yokohama, Kanagawa, Japan.
[2]Department of Environmental Science, Graduate School of Science, Ibaraki University, Mito, Japan.
[3]Research Center for Advanced Science and Technology, University of Tokyo, Tokyo, Japan.
[4]Now at Center for Climate System Research, University of Tokyo, Tokyo, Japan.

Chemistry Aerosol Radiation and Transport (GOCART) model was used during the Asian Pacific Regional Aerosol Characterization Experiment (ACE−Asia) in spring 2001 [*Chin et al.*, 2003]. Chemical weather forecasts from five CTMs provided information for the flight planning during Transport and Chemical Evolution over the Pacific (TRACE−P) in spring 2001.

[3] Chemical weather forecast systems using regional scale models have a horizontal resolution advantage over global models. Regional chemical weather forecasts were first applied to the POLINAT (Pollution from Aircraft Emissions in the North Atlantic Flight Corridor) 2 project [*Flatøy et al.*, 2000]. The Chemical Weather Forecasting System (CFORS) was used during TRACE−P and the ACE−Asia campaign in 2001 [*Uno et al.*, 2003]. *Uno et al.* [2003] showed that changes in synoptic−scale weather greatly influence continental−scale pollution transport in the spring over East Asia.

[4] This paper describes a newly developed global chemical weather forecasting system based on CHASER (chemical atmospheric general circulation model for study of atmospheric environment and radiative forcing) that can be used to support atmospheric chemistry field campaigns. The model includes radiative and dynamical processes and comprehensive chemical schemes for the troposphere and lower stratosphere. This paper assesses the quality and estimates the value of chemical weather forecasts from the model that was used in flight campaigns. Specifically, the CHASER chemical weather forecast system was used during the PEACE campaign. Section 2 describes the forecast system and section 3 describes the PEACE campaign, respectively. Chemical weather forecasts and their use during the PEACE campaign with an emphasis on CO, are shown in section 4. The European plume and outflow from populated regions such as China simulated by the model are examined in detail. Meridional and seasonal variation in CO are mainly discussed. Section 5 contains the conclusions.

2. Global Chemical Weather Forecasting System

[5] The chemical weather forecast system includes the coupled tropospheric chemistry climate model CHASER, which is described and evaluated in *Sudo et al.* [2002a, 2002b]. Physical and dynamical processes are simulated following the Center for Climate System Research/National Institute for Environmental Study/Frontier Research Center for Global Change (CCSR/NIES/FRCGC) atmospheric GCM [*Nakajima et al.*, 1995; *Numaguti*, 1993; *Numaguti et al.*, 1995]. The CHASER model in this study is based on CCSR/NIES/FRCGC AGCM version 5.7b. Advective transport is simulated with a 4th order flux−form advection scheme using a monotonic Piecewise Parabolic Method (PPM) [*Colella and Woodward*, 1984] and a flux−form semi−Lagrangian scheme [*Lin and Rood*, 1996]. Subgrid−scale vertical fluxes of heat, moisture, and tracers are approximated using a non−local turbulence closure scheme based on *Holslag and Boville* [1993] used in conjunction with the level 2 scheme of *Mellor and Yamada* [1974]. The cumulus parameterization scheme is based on *Arakawa and Schubert* [1974] with several simplifications described in *Numaguti et al.* [1997]. The closure assumption is changed from the diagnostic closure used in *Numaguti et al.* [1997] to a prognostic closure based on *Pan and Randall* [1998], in which cloud base mass flux is treated as a prognostic variable. An empirical cumulus suppression condition introduced in *Emori et al.* [2001] is adopted. Note here that the updraft and the downdraft of chemical species by cumulus convection are included in the model. The large−scale condensation scheme is based on *Treut and Li* [1991], in which subgrid probability distribution of total water mixing ratio in each grid box is assumed as a uniform distribution. Spectral coefficients are triangularly truncated at wavenumber 42 (T42), equivalent to a horizontal grid spacing of about 2.8°. The model has 32 vertical layers that are spaced at about 1−km intervals in the free troposphere and lower stratosphere. The chemical side of the model is based on *Sudo et al.* [2002a, 2003], and includes a detailed online simulation of tropospheric chemistry involving the O_3−HO_x−NO_x−CH_4−CO system and oxidation of NMHCs. The chemical model time step is 10 minutes. The model includes detailed dry and wet deposition schemes and heterogeneous reactions on the surface of sulfate and nitrate aerosols.

[6] In addition to the extensive chemical reactions, forecast runs include tagged CO tracers. Such tracers are emitted normally over selected regions (north and south China, Japan, south Asia, northern America, Europe, and Siberia) and evolved subject to model transport schemes and normal chemical loss processes for CO. Figure 1 shows the CO tracer regions. Anthropogenic surface emissions of CO are taken from the *Streets et al.* [2003] inventory over Asia (except China), and from EDGAR (Emission Database for Global Atmospheric Research) [*Olivier et al.*, 1996] over other regions. Surface CO emissions over China are taken from D. Streets et al. (private communication, 2005). The estimated annual amount emissions over China is 146 TgCO, a figure about 40 TgCO larger than that in *Streets et al.* [2003]. In this study, the timing of CO emission from biomass burning was estimated by using the average of the hot spot data from 1995 to 2001 from Along Track Scanning Radiometer (ATSR) [*Arino et al.*, 1999] for the daily forecast. ATSR hot spot data for 2002 were used in the post−analysis study. Tagged CO tracer is also considered for CO which is chemically produced from the oxidation of 4, isoprenes, and other NMHCs.

[7] Figure 2 outlines the procedure used to produce daily forecasts. Each daily run is fully automated and consists of two parts, a "quasi−real−time" run and forecast runs. The quasi−real−time run is derived from the NCEP final analysis (FNL) data, and steps forward one day at a time as soon as the previous day's data are available. Forecast runs use the NCEP Global Forecast System (GFS) data instead of the NCEP FNL data. The NCEP data are re−gridded from 1.0° × 1.0° to 2.8° × 2.8° in horizontal, and from 24 layers to 32 layers in vertical. The relaxation time for nudging the CHASER model meteorological field to the NCEP meteorological data is 1 day in the free troposphere and lower stratosphere. The relaxation time approaches 0 at the surface in this study. Sea surface temperatures (SST) are based on WMO Distributed Data Bases managed by the Japan Meteorological Agency. Winds from 10 hPa to about 3 hPa are calculated by using dynamical and physical procedures in the CHASER model. They are not nudged

Areas for tagged CO
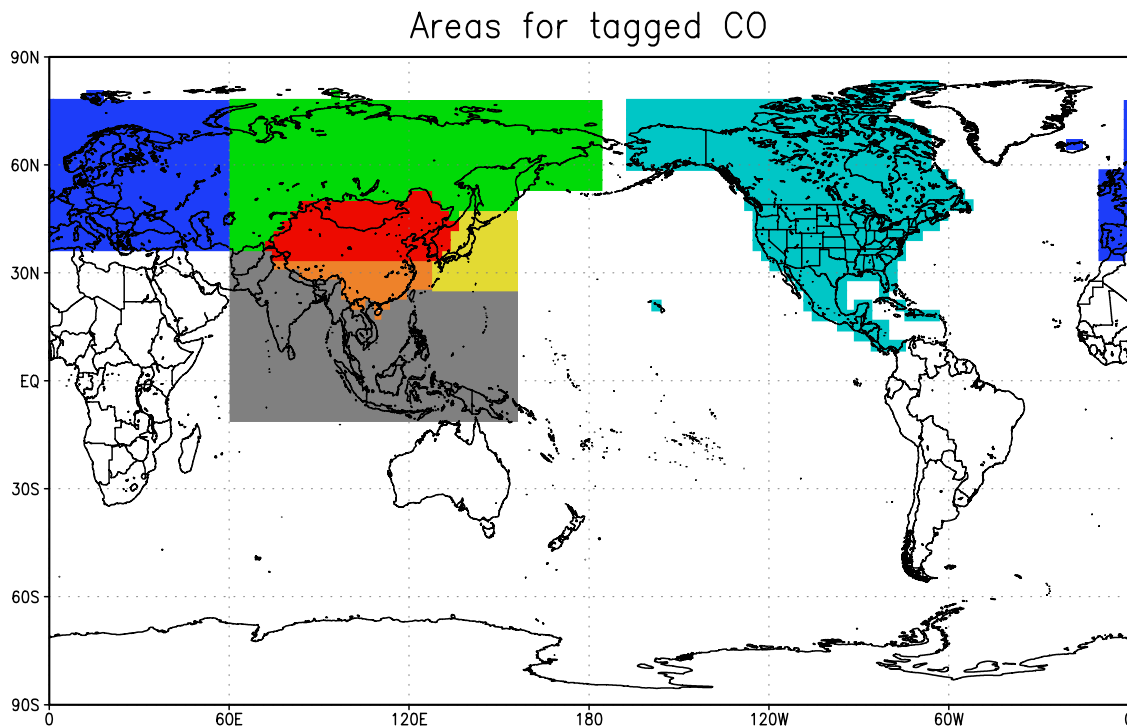
Figure 1. CO tracers regions for CHASER in this study showing European (blue), Siberian (green), northern Chinese and Korean (red), southern Chinese (orange), south Asian (gray), Japan (yellow), and North American (cyan) CO.

by NCEP data because the maximum height of NCEP data is lower than the top of CHASER model. Humidity is calculated using the hydrological cycle (surface source and sink, transport, convection, diffusion, condensation, and precipitation) in the CHASER model. Consequently, the temperature and humidity field do not produce destabilization or discontinuity because of inconsistencies between CHASER temperature and NCEP humidity. The forecast run is initialized from a restart file written at the end of the previous day's quasi−real-time run. Automated runs normally start at 05:00 JST (20:00 UTC of the previous day). Therefore, the 1−day forecast was available for pre−flight briefing during the PEACE campaign. Pre−formatted figures are automatically made from output from both the quasi-real-time and forecast runs. Archived output data can

be used to make custom figures via the web interface (http://www.jamstec.go.jp/frcgc/gcwm).

[8] This forecast system evolved from a prototype run with lower resolution (T21) that started in November 2000. The forecast system then switched to higher resolution (T42) with a spin−up time of 3 months for the global distribution of chemical species. Daily forecasts and archived output data have been available on a web page at the Japan Marine Science and Technology Center (JAMSTEC) since 1 January 2002.

3. PEACE Aircraft Measurement Campaign

[9] The PEACE campaign of the Japan Aerospace Exploration Agency (JAXA) investigated the chemical
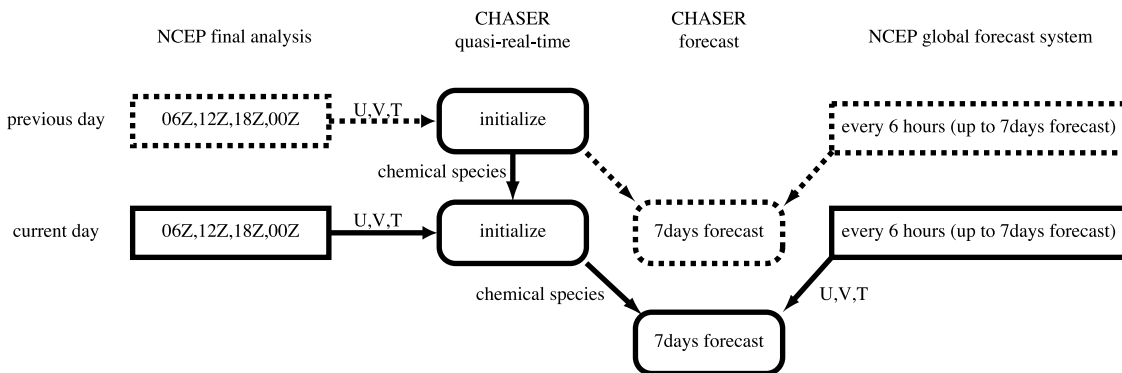
Figure 2. Conceptual representation of the data assimilation for the global chemical weather forecasting system.
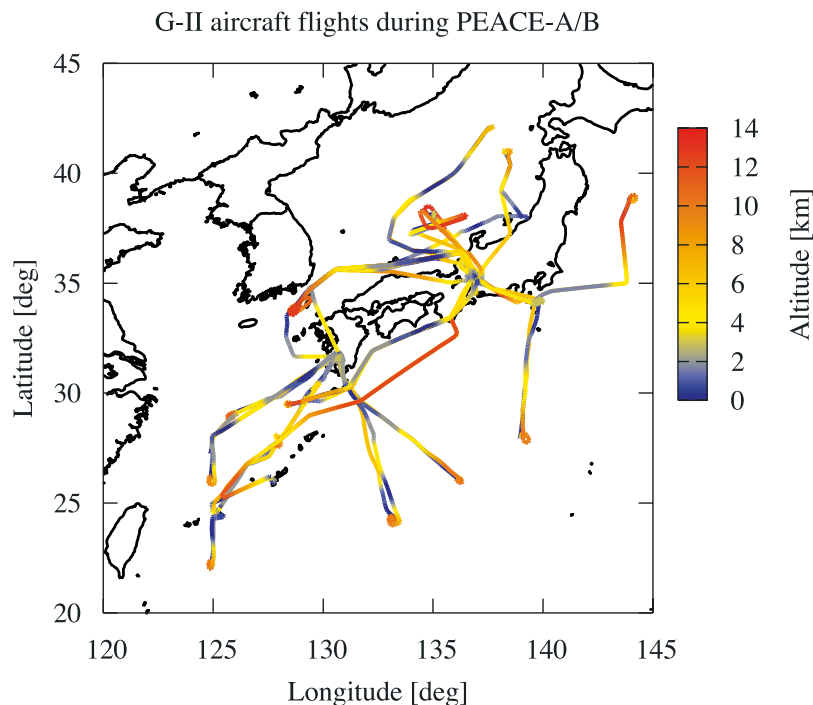
Figure 3. Flight tracks of the Gulfstream II aircraft during the PEACE campaign. The color denotes the altitude.

characteristics of Asian outflow over the western Pacific in winter and spring. These seasons were not covered by PEM−West−B or TRACE−P [cf. *Kondo et al.*, 2004]. The PEACE campaign included two phases. PEACE−A was between 6 and 23 January 2002. PEACE−B was between 21 April and 16 May 2002 in the western Pacific, in association with Intercontinental Transport and Chemical Transformation of Anthropogenic Pollution (ITCT) 2002. A Gulfstream−II (G−II) aircraft from the Mitsubishi Diamond Air Service (DAS) made 25 flights during PEACE. The G−II was based at Nagoya (35.3°N, 136.9°E) during PEACE−A and PEACE−B, and also flew out of Kagoshima (31.6°N, 130.5°E) for some PEACE−A flights. Figure 3 shows the major sampling region. Airborne sampling occurred at altitudes between 0.1 and 13 km. The flights made during PEACE−A and PEACE−B covered latitudes between 22°N and 42°N. Measured quantities included O_3, CO, NMHCs, NO, NO_y, H_2O, $J(NO_2)$, and SO_2. Table 1 of *Parrish et al.* [2004] summarizes the measurement techniques, uncertainties (accuracy and precision), and time resolutions during the PEACE campaign.

[10] The PEACE campaign was designed to investigate seasonal variation in the mode of horizontal and vertical transport and its effect on the distributions of ozone precursors and aerosols in the North Pacific troposphere, to quantify seasonal variation of the oxidizing capacity and ozone budget over the western North Pacific, and to characterize the chemical composition of air masses approaching Japan.

4. Results

[11] The climatological and seasonal distributions of chemical species (i.e., the chemical climate) calculated by CHASER have already been evaluated in *Sudo et al.* [2002b, 2003]. The focus here is on the validation and interpretation of the chemical structures on timescales of hours to days. The targeted features of the flights based on the chemical weather forecasts can be characterized (a) pollution plumes that were affected by intercontinental transport, and (b) the outflow of a polluted air mass from nearby populated regions.

[12] The global chemical weather forecast can predict anywhere where enhanced mixing ratios may occur on a day−to−day bias. However, such predictions would benefit from global or regional model forecasts with higher resolution, especially if they are used to plan flight paths.

4.1. Meteorological Fields

[13] An accurate characterization of transport processes is of critical importance to flight planning and to the analysis of observations. Figure 4 compares PEACE G−II observations of meteorological parameters (wind direction, wind speed, air temperature, and relative humidity) with CHASER meteorological output. Model output was extracted along the G−II aircraft flight path and compared to aircraft observations averaged over 60 seconds. The color of each dot denotes the hight. Wind speed, and air temperature well agreed with the G−II measurements. The modeled relative humidity had a wet bias in the low−humidity regions of the figure. In addition, the model did not reproduce the supersatulated air seen in flight 12 of PEACE−A on 21 January and flight 11 of PEACE−B on 15 May. The flight paths on these dates passed through a low−pressure system, and the coarse resolution of the model failed to resolve fine structures. By same reason, the model could not capture the wind direction in the lower troposphere (red dots in Figure 4), especially in PEACE−B. The correlation coefficients be-
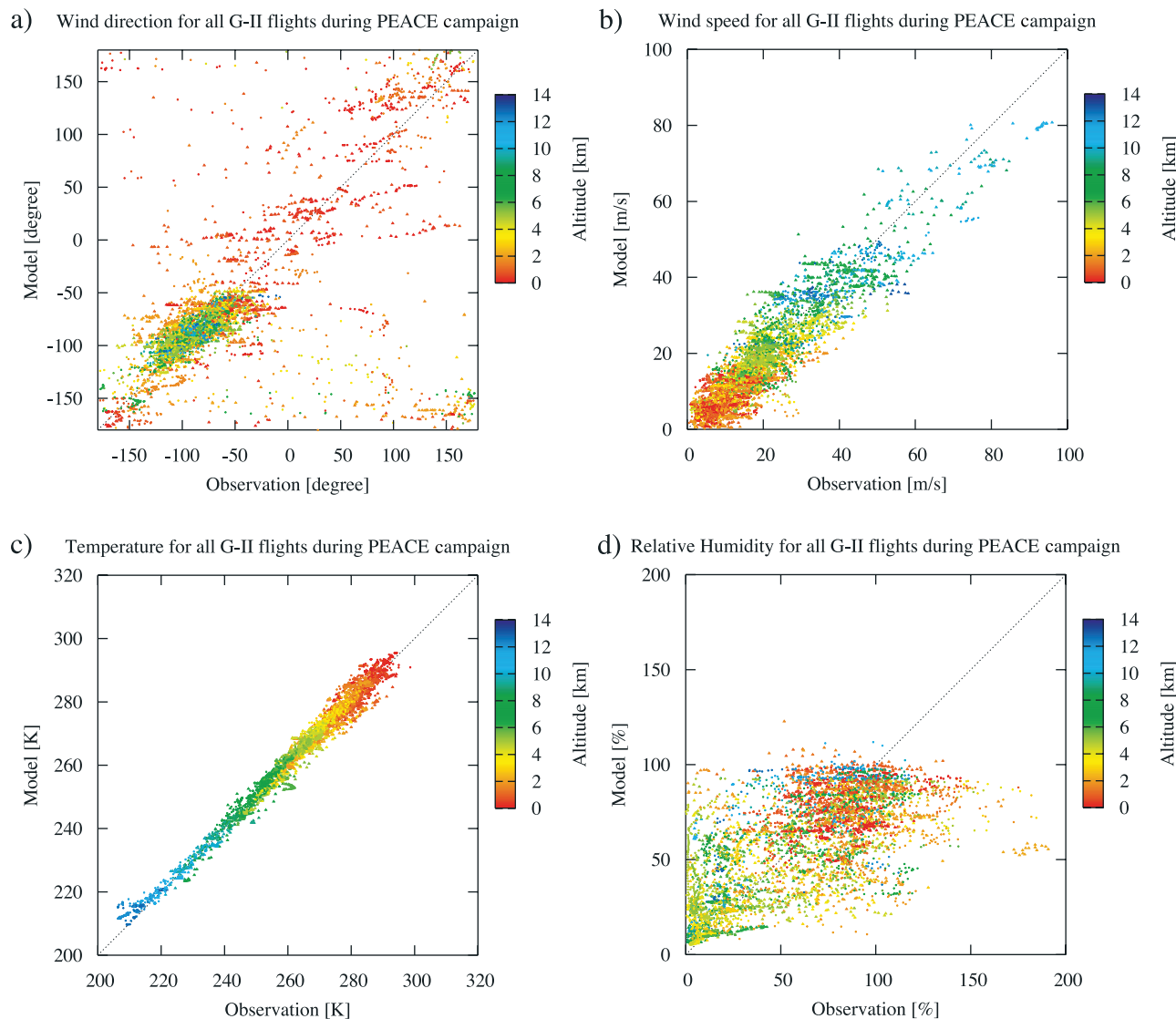
Figure 4. Comparison between PEACE G–II airborne meteorological parameters and global chemical weather forecasting system output fields along the flight paths. Red and blue color denote observations and model output, respectively. Dots and crosses denote PEACE–A and PEACE–B data, respectively.

tween model data and observation for all G–II flights were 0.81, 0.91, 0.99, and 0.66 for wind direction, wind speed, temperature, and relative humidity, respectively. The CHASER global chemical forecasting system accurately captured many of the important observed meteorological features during PEACE. The results presented here are driven by the NCEP FNL data. The forecast and hindcast meteorological fields were similar during both PEACE–A and PEACE–B.

4.2. Comparison With Ground–Based Observations

[14] The mixing ratios of chemical species calculated by the chemical weather forecasting system during PEACE were compared with values observed at three ground–based observational sites in the major sampling region of PEACE. Figure 5 shows CO at Minamitorishima (24.2°N, 153.6°E), Yonagunijima (24.3°N, 123.1°E), and Ryori (39.2°N,

141.5°E). The model reproduced the observed temporal variations of each site except small peaks at Yonagunijima, especially in winter. Although biomass–burning emissions based on the 2001/2002 ATSR hot spot data were incorporated into the model, the model still underestimated CO mixing ratio by about 20 ppbv at these sites in spring. The hot spot data correlated well with emission anomalies, especially for Siberia [*Yurganov et al.*, 2005]. The 2002 Siberian fire season, which started early, was a significant source of the pollution observed over the northeast Pacific in May [*Bertschi et al.*, 2004]. A possible reason for the underestimation of the CO mixing ratio is that the model does not simulate biomass–burning emissions from smoldering. Underestimates of CO in spring may also arise from overestimates in the reaction of CO with. The modeled CO loss in May was about 10% larger than those modeled by MATCH–MPI [*von Kuhlmann et al.*, 2004]. It should be

Figure 5

a)

O3 at Minamitorishima [24.18N,153.58E,8m]

b)

O3 at Yonagunijima [24.28N,123.1E,30m]

c)

O3 at Ryori [39.2N,141.49E,260m]
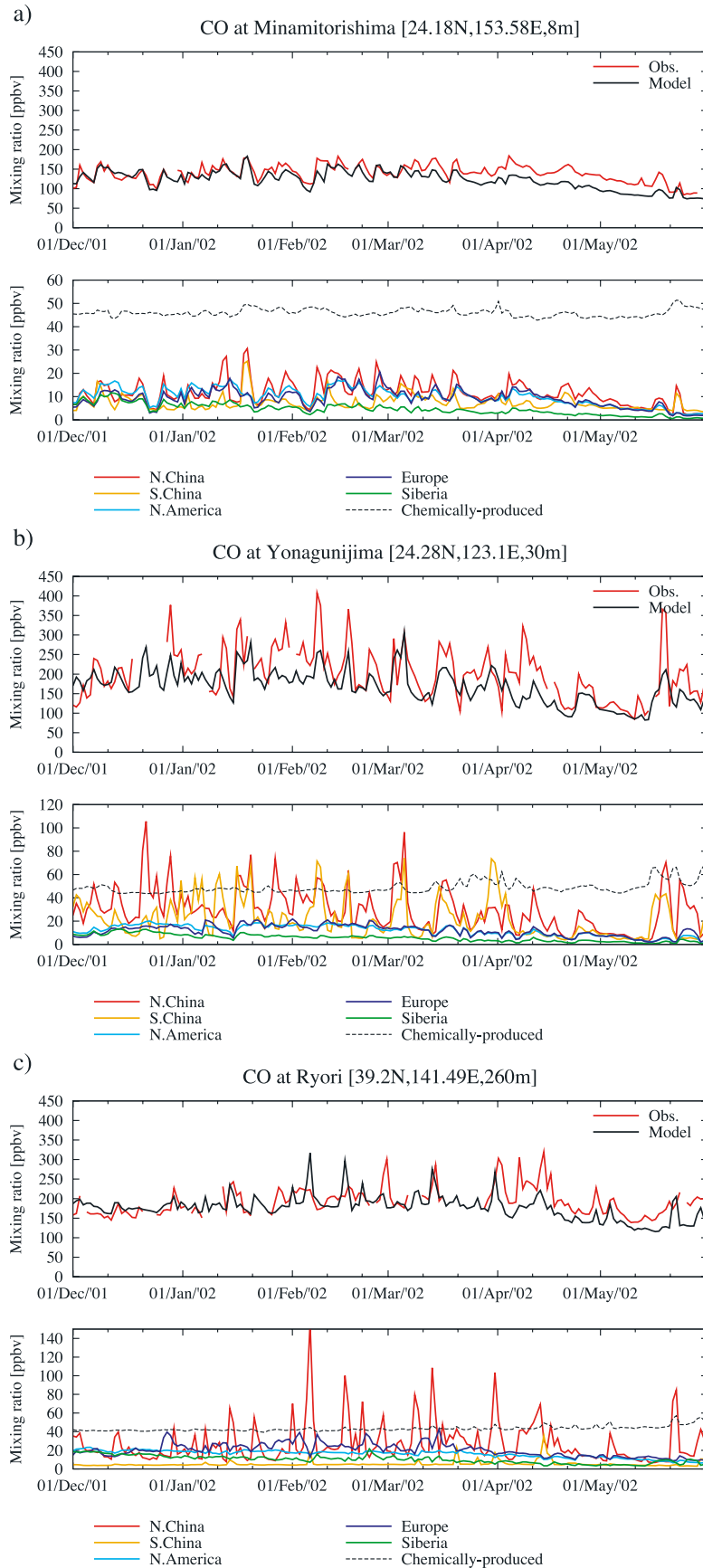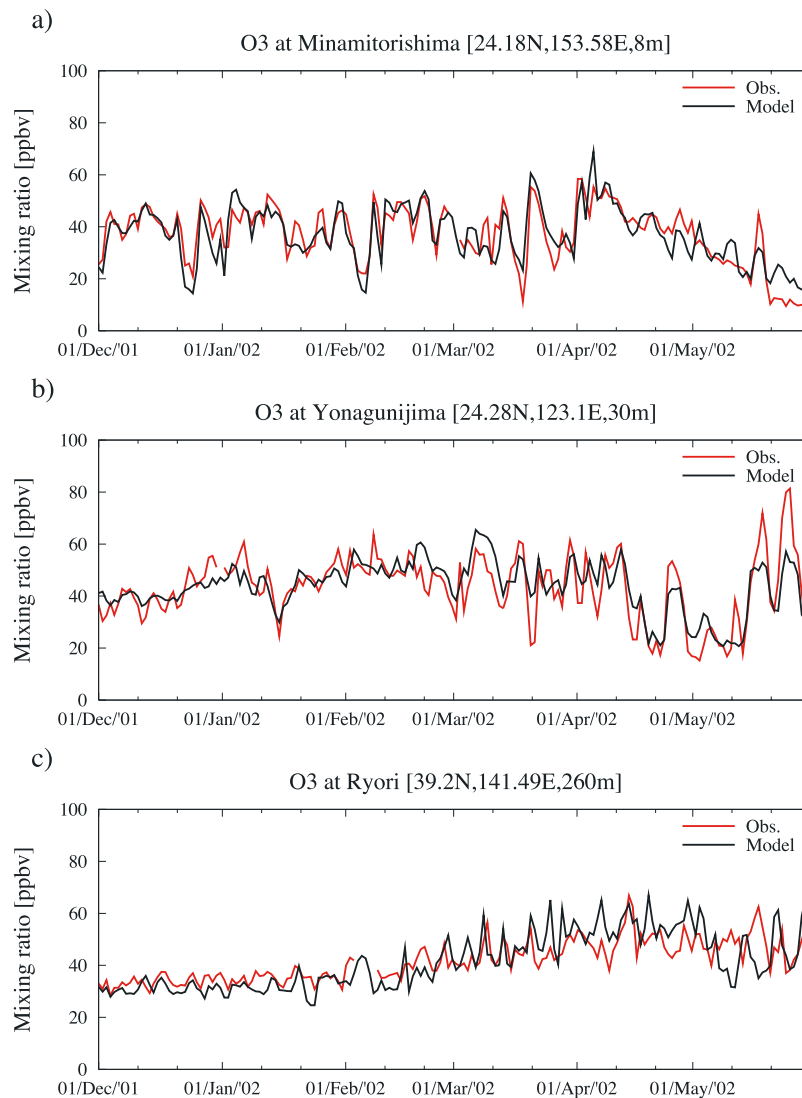
Figure 6. As in Figure 5, but for ozone.

noted here that the reaction rate of the reaction of CO with is taken from [*McCabe et al.*, 2001] for the present version of the model. The uncertainty of this reaction is supposed to be about 10% [*Cox et al.*, 2005], and the modeled CO loss in May was decreased by 5% when the reaction rate of this reaction was decreased by 10%.

[15] Figure 5 also shows the regional CO tracers calculated by CHASER. Siberian CO made small contribution to the CO concentrations in late spring at these sites. The concentration of Siberian CO does not exceed 5 ppbv in late spring. Minamitorishima is in the southeast of Japan and is affected by maritime air and outflow from Asia. Tagged CO tracers suggest that the enhanced CO level observed at Minamitorishima on 18 January are linked to emissions

from northern and southern China. The CO levels at Yonagunijima are strongly related to the Asian CO tracers. Some events with increased CO levels greater than 300 ppbv occurred at Yonagunijima. Corresponding increases occurred in the China CO tracers in such events. Tracers of CO that is chemically produced from the oxidation of CH_4, isoprenes, and other NMHCs, increased by about 5–10 ppbv in the CO increase event in the spring. Increases in CO tracers linked to chemical production from hydrocarbons in polluted air masses reflect the enhanced chemical activity in the spring.

[16] Figure 6 shows the temporal evolution of surface ozone at the same sites as in Figure 5 from December 2001 to May 2002. The model reproduced the observed seasonal

Figure 5. Observed (red lines) and modeled (black lines) surface CO mixing ratio at (a) Minamitorishima (24.2°N, 153.6°E), (b) Yonagunijima (24.3°N, 123.1°E), and (c) Ryori (39.2°N, 141.5°E). Regional tagged CO tracers for northern China and Korea (red), southern China (orange), south Asia (gray), Europe (blue), North America (cyan), and chemically production (dotted lines) are also shown.

Table 1. Statistical Comparison of Observations at WDCGG Sites With the Model Results

	Species	r	RMS$_c$[a]	R_{ave}[b]	R_σ[c]
Minamitorishima	CO	0.76	0.11	0.88	1.10
	O$_3$	0.84	0.17	0.99	0.95
Ryori	CO	0.53	0.18	0.90	0.90
	O$_3$	0.73	0.18	1.00	1.41
Yonagunijima	CO	0.71	0.23	0.84	0.66
	O$_3$	0.78	0.18	1.01	0.78

[a]Centered root mean squares.
[b]Ratio of the modeled values to the observed mean mixing ratios.
[c]Ratio of the standard deviations ($\sigma_{model}/\sigma_{observation}$).

evolution of surface ozone at all of the sites. For example, the observations and model output both show a monotonic decrease in ozone in May at Minamitorishima, an increase in May at Yonagunijima, and a spring maximum at Ryori.

The amplitude of the increase in May at Yonagunijima was slightly underestimated in the model.

[17] Table 1 shows statistical comparisons of modeled and observed surface ozone and surface CO at the three ground−based observational sites during PEACE. The model results correlate well with the observations. The correlation coefficients exceed 0.5, reaching as high as 0.84. The root−mean−square (RMS) differences show that the modeled values were generally within 10−20% of the observed values. The ratio of averaged values suggests that the model underestimates the CO mixing ratios by 10−16%. The standard deviation of CO in the model is within 10% of the observed CO standard deviation at Minamitorijima and Ryori. Yonagunijima, located southwest of Japan, is more strongly affected by the influx from China. Although the model reproduced the temporal pattern of the polluted air masses at Yona-
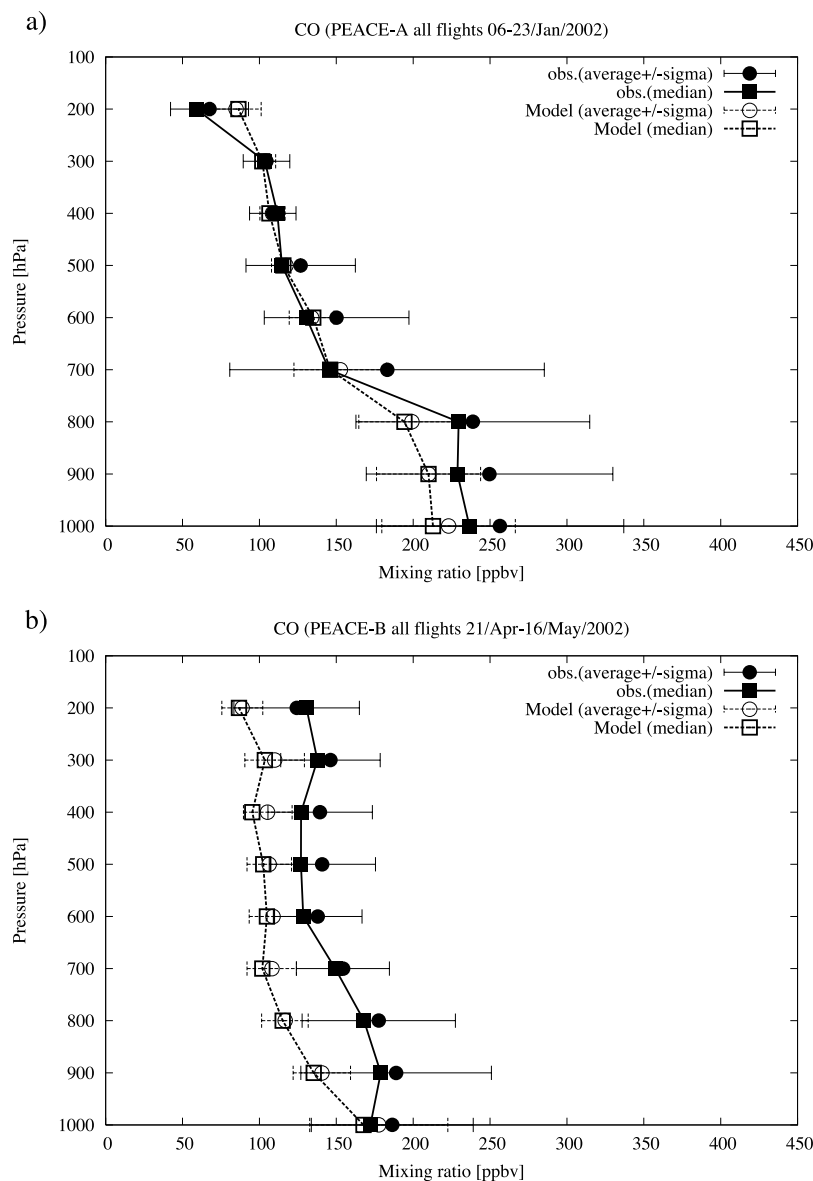
Figure 7. (a) Vertical profiles of CO calculated by CHASER and airborne observations from PEACE−A. (b) As in Figure 7a, but for PEACE−B. Circles denote the average, squares denote the median, and horizontal bars denote 10th and 90th percentiles, respectively.
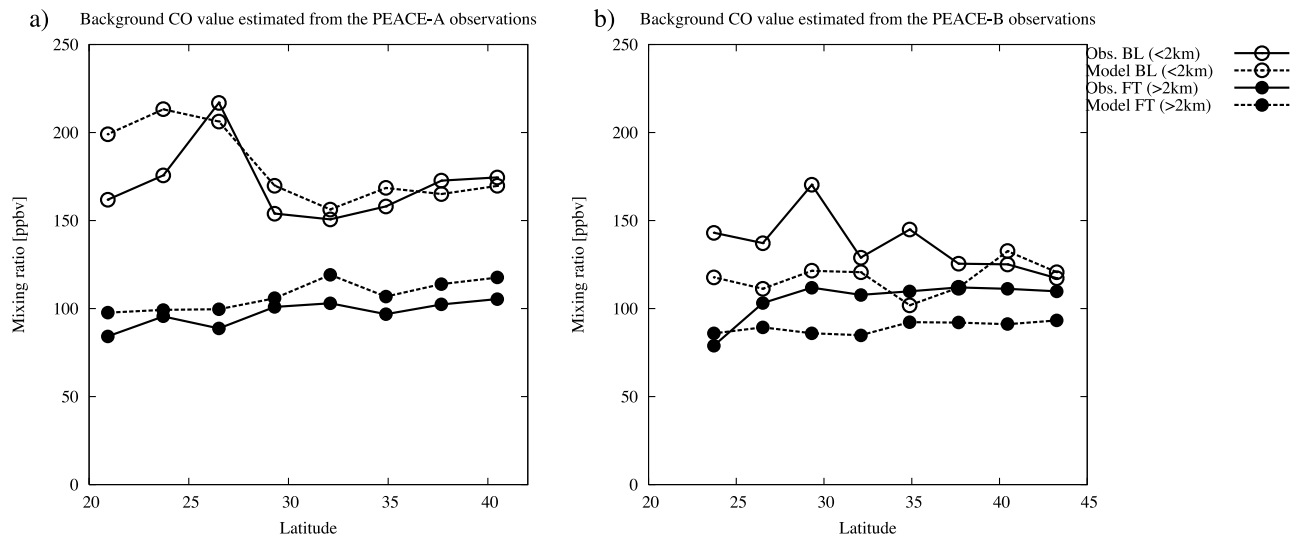
Figure 8. (a) Background CO values estimated during PEACE−A as a function of latitude for the lower troposphere (from the surface to 2 km, open circles) and the free troposphere (from 2 to 12 km, black circles). Background values are evaluated by calculating the 10th percentile of observations for each latitude and altitude bin. Dotted lines denote the 10th percentile of the model calculations. (b) As in Figure 8a, but for PEACE−B.

gunijima (Figure 5b), plume values were underestimated because of the coarse model resolution.

4.3. Comparison With Airborne Observations

[18] This section compares model results with airborne observations during PEACE. Figure 7 compares a flight track−mean CO vertical profiles constructed from PEACE−A and PEACE−B observations and includes mean CO vertical profiles derived from output from the CHASER chemical weather forecasting system, which are extracted along flight tracks of the respective campaigns. Both simulations use 2001/2002 ATSR hot spot data as a scaling factor of biomass−burning emission inventories. Although the model CO has a negative bias of about 20 ppbv in the boundary layer, the model calculations still agree with PEACE−A observations. The modeled CO concentration in the free troposphere (FT) is generally within 5 ppbv of the observed vertical profile. The model CO agrees with surface observations during PEACE−B. The model CO has a negative bias of 20−50 ppbv above 900 hPa.

[19] The distributions of the ΔCO concentrations are estimated to evaluate the model's ability to reproduce transport processes associated with synoptic−scale weather patterns regardless of model biases in the CO concentration. Δ is defined as the increase in concentration over the background concentration. The background CO concentration is estimated in each model latitude bin (about 2.8°) over the PEACE region by computing the 10th percentiles for the observed values in the lower and upper troposphere. The background CO concentration is characterized by strong latitudinal and vertical variation that reflects sources in the northern mid−latitudes, the structure of the continental outflow, and the meridional and vertical variation in photochemical sinks. Stratospheric air masses are identified from the diagnosis of the tropopause in the CHASER temperature field, which are nudged by the NCEP reanalysis data.

Figure 8 shows the estimated background CO mixing ratios during PEACE. The dotted lines show the 10th percentile from the model calculations in each meridional model bin. The modeled CO has a negative bias of 20 ppbv in the free troposphere (FT); this model bias shows little meridional variation. There are only 11 observation points in the FT in the southernmost bin, so the difference in the southernmost bin is not included in the statistical comparison in Table 2.

[20] Table 2 shows statistical comparisons between ΔCO derived from model output and from airborne observations during PEACE. *Kiley et al.* [2003] compared the output from four state−of−the−art global chemical transport models with the TRACE−P observations and found that the correlations between the model and observations ranged from 0.56 to 0.75, which generally agrees with the correlations for the model output and observations during PEACE except in the lower troposphere (LT) during PEACE−B period. The standard deviation in the model is about half of that observed in PEACE−A. The global model cannot reproduce plumes with the highest concentration of CO. The calculated ΔCO correlates well with observations in PEACE−A in the lower and free troposphere: the correlation coefficients exceed 0.5. Although the model reproduced the pollution plumes observed during

Table 2. Statistical Comparison of ΔCO Estimated From the CHASER Model and 60−s Averaged Observed Values in the PEACE Campaign

		Points	r	RMS_c	R_σ
PEACE−A	LT(<2 km)	1071	0.53	0.84	0.47
	FT(>2 km)	1495	0.63	0.95	0.53
	Stratosphere	47	0.87	0.89	0.66
PEACE−B	LT(<2 km)	721	0.09	1.47	0.80
	FT(>2 km)	1853	0.49	0.92	0.47
	Stratosphere	38	0.36	1.30	0.10
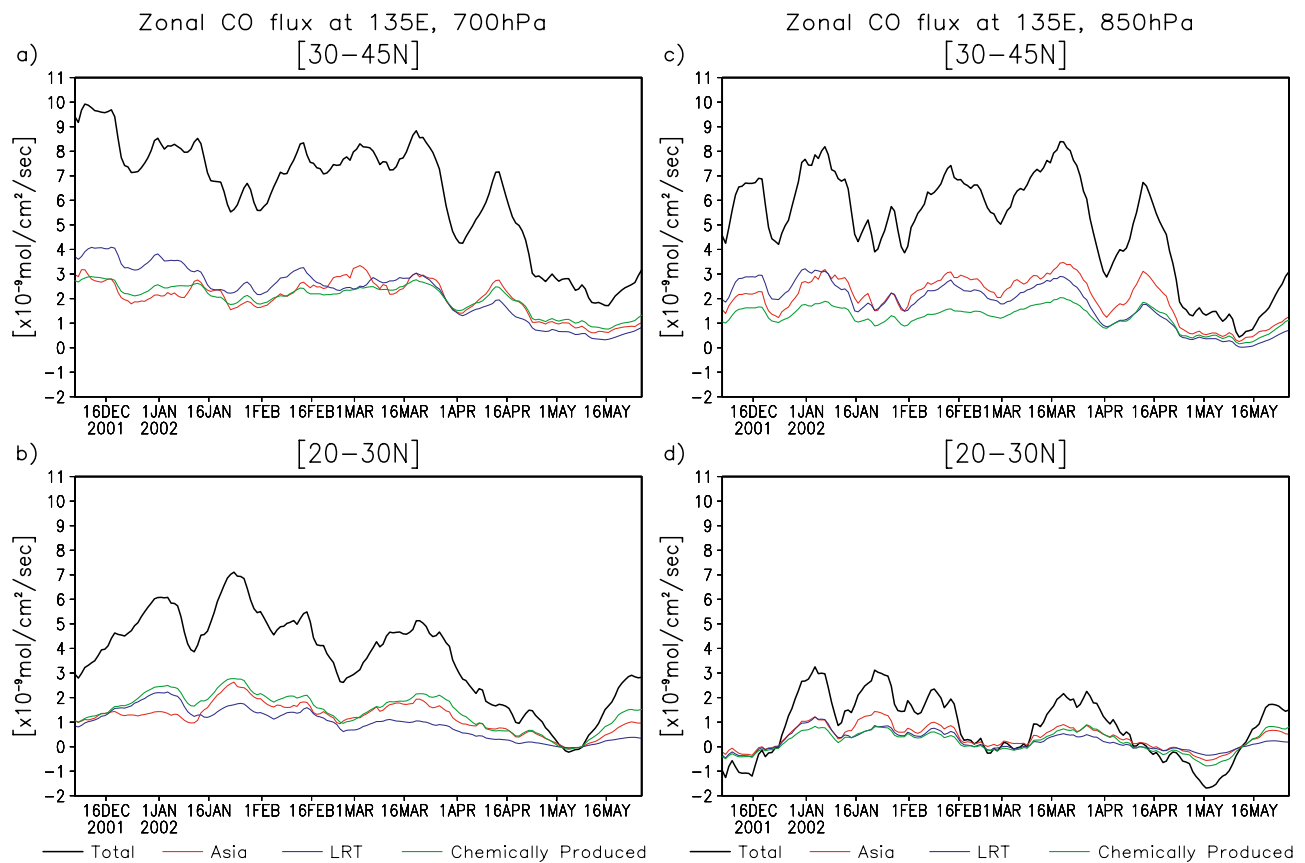
Figure 9. Ten−day running mean of the model calculated daily CO flux over 135°E for 2001 December to May 2002. (a) At 700 hPa, averaged for 30°−45°N. (b) At 850 hPa, averaged for 30°−45°N. (c) At 700 hPa, averaged for 20°−30°N. (d) At 850 hPa, averaged for 20°−30°N. The units are mol/cm²/sec. Positive values correspond to eastward transport, and negative values correspond to westward flux. The black, red, blue, and green lines denote total CO flux, Asian anthropogenic and biomass−burning CO flux, long−range transported CO, and chemically produced CO from CH_4, isoprenes, and other NMHCs, respectively.

PEACE−A, the model concentrations are diluted because of the coarse model grid. The model failed to reproduce the distribution of chemical species in the boundary layer in late spring, because of model difficulties simulating turbulent processes in the boundary layer during this period. By applying the non−local turbulence closure scheme, the correlation coefficients between the modeled and observed ΔCO was increased from 0.01 to 0.09 in the LT during PEACE−B. It suggests that the vertical transport from the boundary layer was underestimated in the model, especially in late spring. However, the correlation coefficients between the modeled and observed ΔCO are quite small in the LT during PEACE−B. Therefore, the modeled CO profile in the LT is not compared to airborne observations during PEACE−B.

[21] To evaluate the effect of anthropogenic surface emissions of CO over China based on D. Streets et al. (unpublished data, 2005), additional model calculation was executed by using surface emissions of CO over China based on *Streets et al.* [2003]. The temporal pattern of the polluted air masses from China continent was not affected by the change of surface emissions, and the change of surface emissions over China made small contribution to the

correlation coefficients between modeled and observed CO during PEACE. In contrast, CO concentrations in polluted air masses over Japan were increased by using updated CO emissions over China. The standard deviation of the CO in the model increased from 43 ppbv to 51 ppbv by using D. Streets et al. (unpublished data, 2005). The standard deviation of CO in the observations during PEACE was 75 ppbv. The averaged ratio of modeled to observed CO increased from 0.76 to 0.80 by using updated surface emissions of CO over China. The model results were improved by using updated surface emissions over China, but the model still underestimated CO levels in late spring.

4.4. Long−Range Transport of Plumes During the PEACE Campaign Calculated by the 3−D Model

[22] Figure 9 shows the latitudinal averaged zonal CO flux at 135°E from December 2001 to May 2002, the period corresponding to PEACE. Positive (negative) values mean the eastward (westward) transport. The fluxes of the Asian CO, long−range transported (LRT) CO, and chemically produced CO are also shown. The units are mol/cm²/sec. The Asian CO includes all tagged CO from anthropogenic and biomass burning emissions over northern and southern
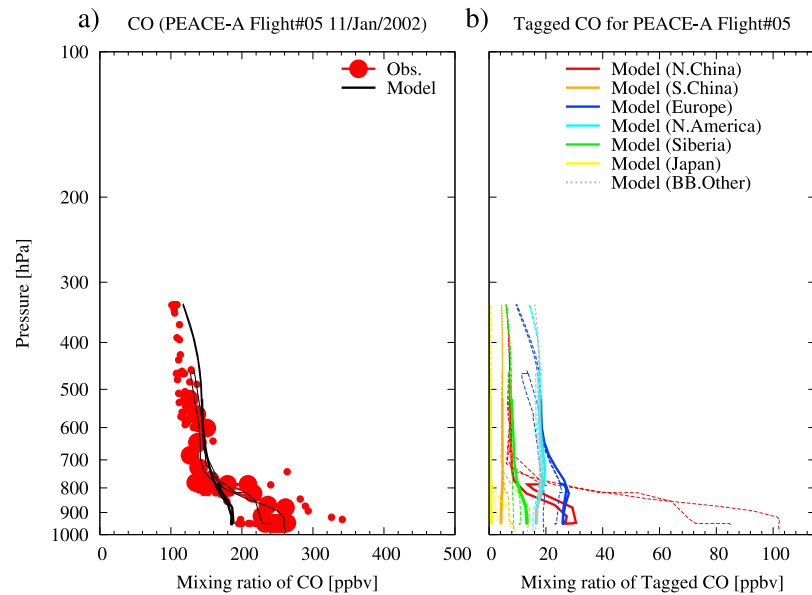
Figure 10. (a) Vertical profiles of the observed CO mixing ratios (red circles), along with the model output corresponding to the flight tracks for PEACE−A flight 5 on 11 January. Black line denotes the total CO calculated by CHASER. (b) Regional tagged CO tracers for northern China and Korea (red), southern China (orange), Europe (blue), North America (cyan), Siberia (green), Japan (yellow), and biomass−burning outside from Asia (gray). The bold lines indicate CO values from 8:03 UTC to 8:37 UTC.

China, Japan, and southern Asia. The LRT CO sums the CO tracers from anthropogenic and biomass−burning emissions outside of Asia. Chemically produced CO arises from the oxidation of 4, isoprenes and other NMHCs. The CO outflow to the Pacific is about twice as large over Japan (30°−45°N) as over the regions south of Japan (20°−30°N). The contributions of LRT CO to the CO outflow are relatively large in winter. A typical case occurred between 20 December 2001 and 10 January 2002 at 30°−45°N in the

FT and LT (Figures 9a and 9c). Over southern Japan (Figures 9b and 9d), chemically produced CO plays an important role in Asian CO outflow.

[23] Several flights were made during the period of increased LRT CO during PEACE−A. Figure 10 shows the vertical profiles of the CO mixing ratio along the track of flight 5 on 11 January 2002 during PEACE−A. Figure 10 includes 60−second averaged observations and the model output extracted along the flight track. The correlation
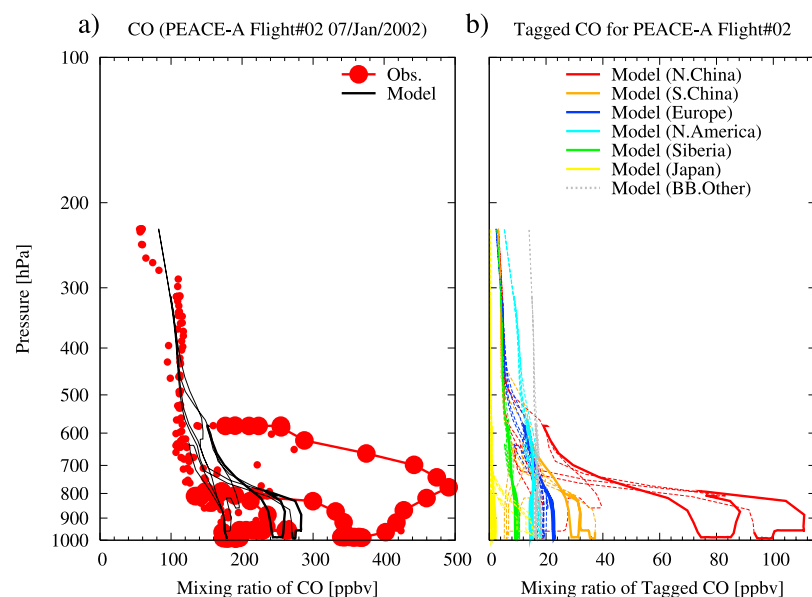
Figure 11. As in Figure 10, but for flight 2 on 7 January 2002. The bold lines indicate CO values from 3:53 UTC to 4:27 UTC and from 5:17 UTC to 5:42 UTC.
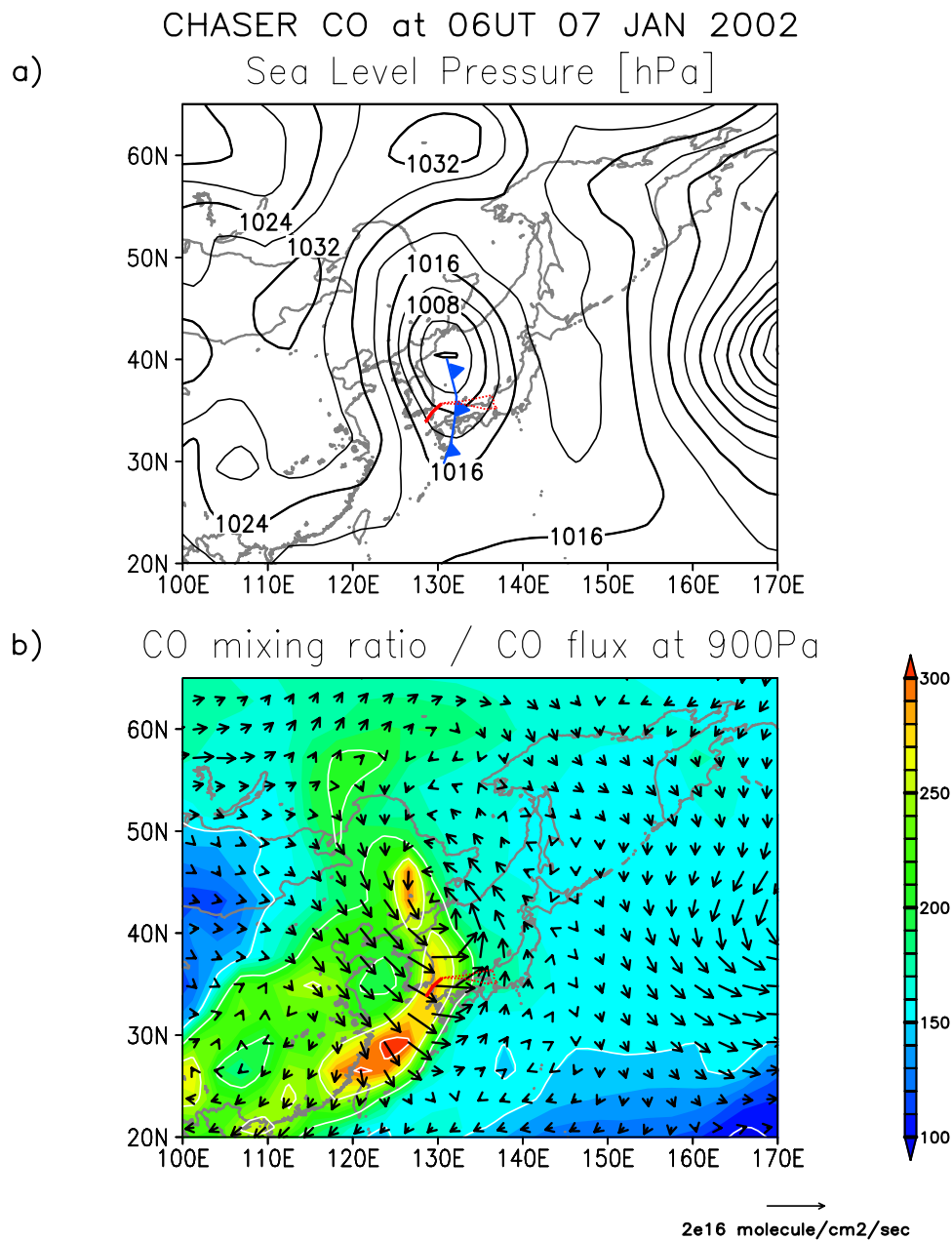
Figure 12. (a) Sea level pressure at 06:00 UTC on 7 January 2002. The contour interval is 4 hPa. (b) CO mixing ratio at 900 hPa. The contour interval is 50 ppbv. Arrows denote the CO flux at 900 hPa. The unit length is shown below the figure. Red lines denote the path of flight 2 during PEACE−A, and the legs from 3:53 UTC to 4:27 UTC and from 5:17 UTC to 5:42 UTC are shown with the bold lines.

coefficient between the observed and calculated CO for flight 5 is 0.78. The average relative RMS error of the model CO to the observed CO is 20% and the mean ratio of the model CO to the observed CO is 0.68. CHASER overestimated the mean CO levels in the free troposphere, but the model did reproduce well the trace gas distributions for this flight. Regional tagged CO tracers which have the values exceeding 5 ppbv are also shown in Figure 10. European CO during flight 5 was widespread in the upper troposphere, with an estimated mixing ratio of 20 ppbv in the free troposphere, and 20−27 ppbv in the boundary layer. North American CO and biomass burning CO from regions outside Asia also made large contribution to the CO con-

centrations in the free troposphere during this flight. Asian CO, including Chinese CO, showed small concentrations in the free troposphere during this flight. By contrast, CO from northern China dominated in the boundary layer, where CO concentrations in the polluted plume exceed 100 ppbv. Tagged CO tracers suggest that CO from northern China comprises 68% of this LT plume.

4.5. Continental Outflow During the PEACE−A Campaign

[24] Two continental outflow events observed during PEACE−A, and the corresponding CHASER simulations, can be used to illustrate transport pathways and the con-
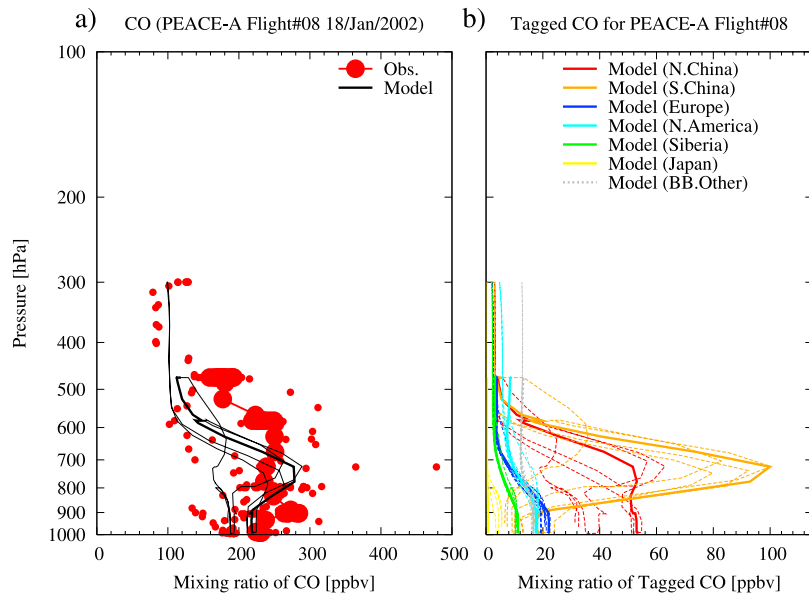
Figure 13. As in Figure 10, but for flight 8 on 18 January during PEACE−A. The bold lines indicate CO values from 4:27 UTC to 5:17 UTC.

tributions from each tagged CO tracer. The first event occurred in an airstream behind a cold front in the lower troposphere, corresponding to flight 2 of PEACE−A on 7 January 2002. Strong subsidence constrained the post

cold front (PCF) airstream to 0−2 km altitude. High pollutant concentrations have been observed in the air masses of PCF airstreams in NARE '97 and TRACE−P [*Cooper et al.*, 2001; *Liu et al.*, 2003]. The second
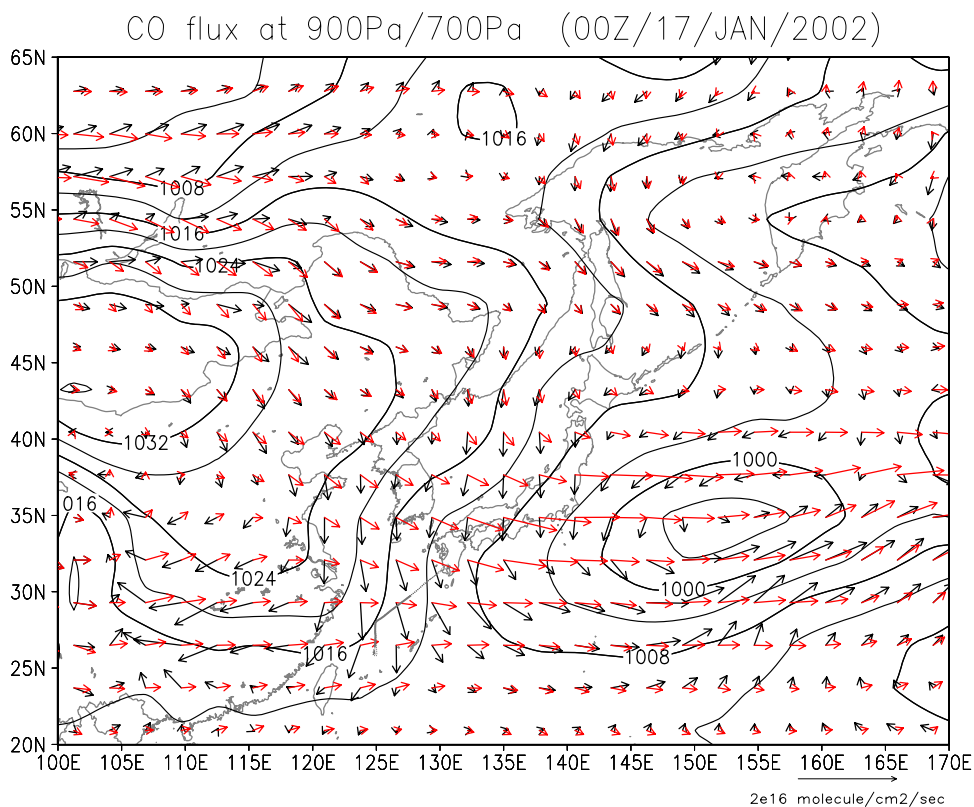
Figure 14. The CO flux at 900 (black arrows) and 700 hPa (red arrows) at 00:00 UTC 17 January 2002. The unit length is shown below the figure. Contours denote sea level pressure. Red line denote the path of flight 08 during PEACE−A, and the leg from 4:27 UTC to 5:17 UTC is shown with the bold line.
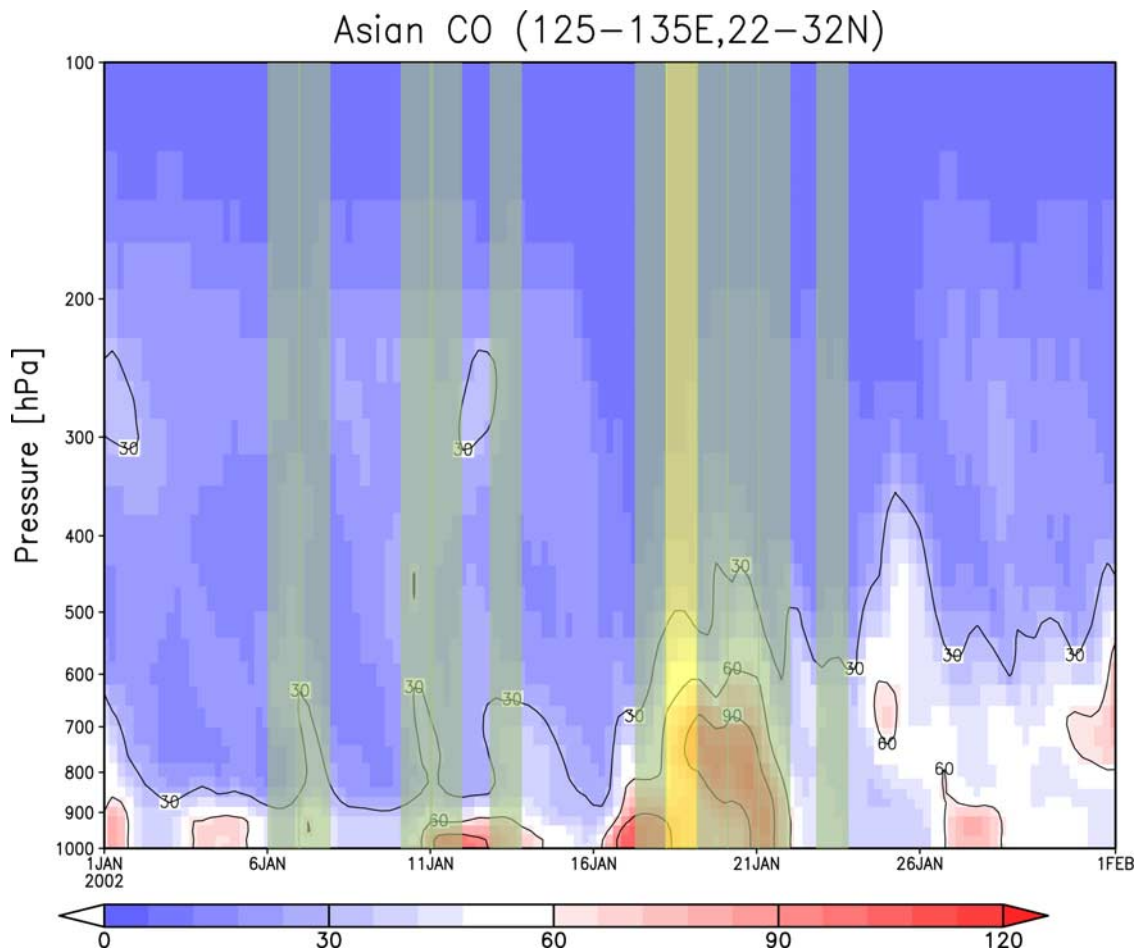
Figure 15. Time−pressure cross−section of the mixing ratio of Asian CO in January 2002 calculated using CHASER. The contour interval is 10 ppbv. The values are averaged over the area for 125°−135°E and 22°−32°N. Shaded regions denote PEACE−A flights, and yellow regions denote flight 8 during PEACE−A campaign.

example is characterized by large vertical wind shear in the lower and free troposphere and was sampled by flight 8 of PEACE−A on 18 January 2002.

[25] Figure 11 shows the observed and modeled vertical profiles of the CO mixing ratio in flight 2 of PEACE−A on 7 January 2002. The observed and modeled vertical profiles show an enhanced CO mixing ratio in the lower troposphere. The observed increase is from values of about 180 ppbv outside the plume to over 400 ppbv in the plume. The modeled increase is smaller, from values of 180 ppbv to 260−290 ppbv, and is limited to heights below 800 hPa. However, the model clearly captures a plume signal in this flight (see also Figure 12). Tagged CO tracers suggest that the enhanced CO in the LT plume originated from emissions over northern China. Indeed, CO from northern China accounts for 35−38% of the total CO in the plume and CO from southern China accounts for 11−13% of the plume. Figure 12 shows the sea level pressure, modeled CO fluxes at 900 hPa, and modeled CO mixing ratio at 900 hPa at 12:00 UTC on 7 January 2002. A synoptic−scale mid−latitude cyclone was in the east of the Korean Peninsula, and a cold front was between 132°E, 38°N and 130°E, 30°N (Figure 12a). The maximum CO flux at 900 hPa is south of the cyclone. The CO flux is northwesterly behind the cold front. There is a plume of pollution in the west of Japan, corresponding to and area of CO flux convergence in the LT. The modeled CO concentration in the plume exceeds 250 ppbv (300 ppbv in maximum), and this concentration is about 100 ppbv higher than the background level during PEACE−A, as estimated in section 4.3 (150 ppbv for 32°N in LT).

[26] Figure 13 shows vertical profiles of the CO mixing ratios along the track of flight 8 during PEACE−A. The observed and modeled vertical profiles indicate that there is more CO in the middle troposphere (MT) than in the LT and UT during this flight. The CO concentrations are enhanced between 500−800 hPa. The observed enhancement is near 200 ppbv in this flight. The modeled CO concentration enhancement is weaker (50−100 ppbv), and the model does not reproduce the thin layer of enhanced CO observed around the 700 hPa level. However, the model shows clear plume signatures during the period when the enhanced values were measured. Tagged CO tracers show that the enhanced MT CO concentrations during this flight arise from Asian CO. The ratio of Asian CO tracers to total enhanced CO in the MT is 23−31%. Figure 14 shows the sea level pressure and CO fluxes at 700 hPa and 900 hPa at 00:00 UTC on 17 January 2002. An anti−cyclone splits in
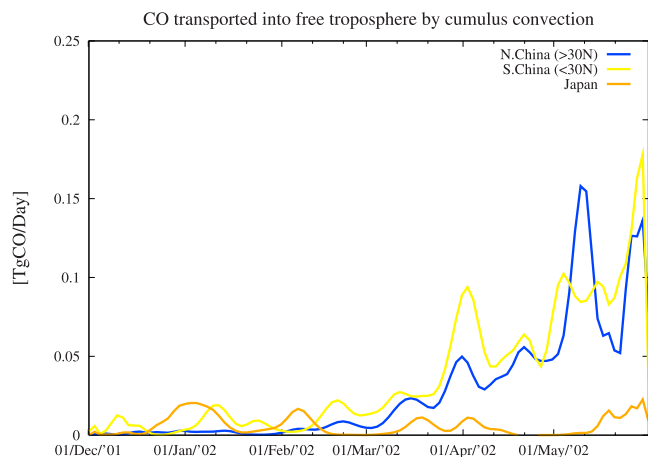
Figure 16. Ten−day running mean of CO transported by convection over northern China (blue line), southern China (yellow line), and Japan (orange line) during PEACE as calculated by CHASER. The units are TgCO.

two as it passed over Japan on 14 January. Therefore, a strong vertical wind shear persisted from 15 to 18 January. The CO flux in the LT is northerly or northwesterly over, and the CO flux in the MT is westerly over the East China Sea. Figure 15 shows a time−pressure cross−section of the mixing ratio of Asian CO tracers in January 2002 calculated from CHASER. The values are averaged over western Japan, corresponding to typical flight paths from Kagoshima during PEACE−A. A concentrated plume of Asian CO in MT is present from 18 to 21 January. The values of the plume are over over 90 ppbv as the mean values averaged over the 2.8° latitude and 2.8° longitude region. The value of Asian CO in LT is about 60 ppbv on 17 January 2002. Because of the vertical wind shear and the northwesterly

CO flux, the CO level in LT is related to the north Chinese CO.

4.6. Convective Outflow During the PEACE−B Campaign

[27] Convective activity can play an important role in late spring, when PEACE−B was conducted. *Oshima et al.* [2004] evaluated the origin of air parcels sampled by the aircraft during PEACE−B from altitudes between 4 and 13 km using back trajectories and estimated that 69% of those air parcels that originated at or below 800 hPa experienced convective uplifting.

[28] CCSR/NIES/FRCGC AGCM and CHASER consider tracer updraft and downdraft corresponding to deep cumulus convections. Figure 16 shows the modeled mass change of CO tracers in the free troposphere (above 2 km) caused by convective transport over northern China (poleward of 30°N) and Korea, southern China (equatorward of 30°N), and Japan. The model results show greater vertical transport resulting from deep convection over China in late spring. A clear increase also occurs in January over Japan. The increase over Japan is related to the passage of mid−latitude cyclones over Japan. The monthly budget of convective transport for May is estimated to be about 3 TgCO over northern China, and about 3.3 TgCO over southern China. These values are about half of all the surface emissions over China in May: The monthly budget of surface emissions in the model over northern and southern China in May is about 6.5 TgCO and 6.4 TgCO, respectively.

[29] Several PEACE−B flights were made in May 2002 when convective CO transport was active. Figure 17 shows the vertical profiles of the observed and modeled CO mixing ratio on 14 May 2002 for flight 10 of PEACE−B. CO increased between 300−400 hPa. The model typically underestimates background CO level by about 20−40 ppbv compared to the PEACE−B observations, but in this flight,
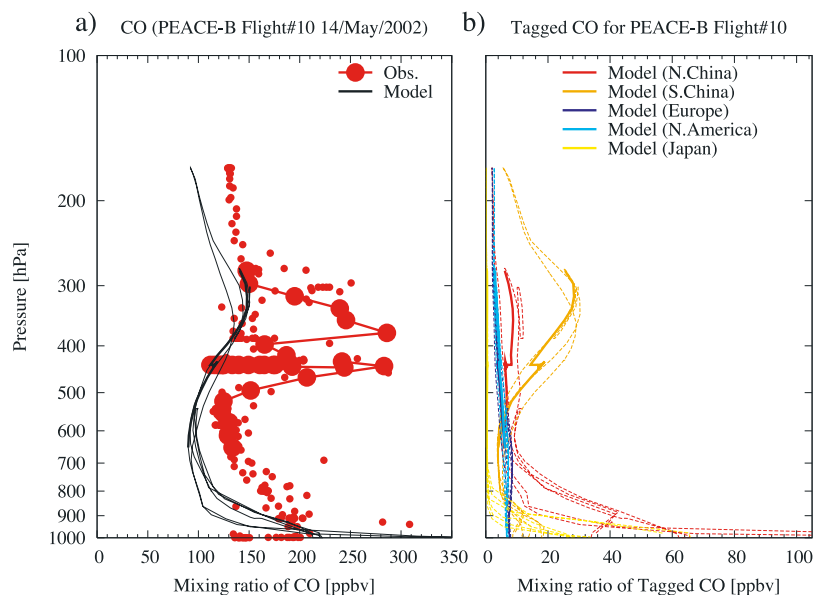
Figure 17. As in Figure 10, but from flight 10 of the PEACE−B campaign on 14 May 2002. The bold line indicates CO values from 6:48 UTC to 7:22 UTC, respectively.
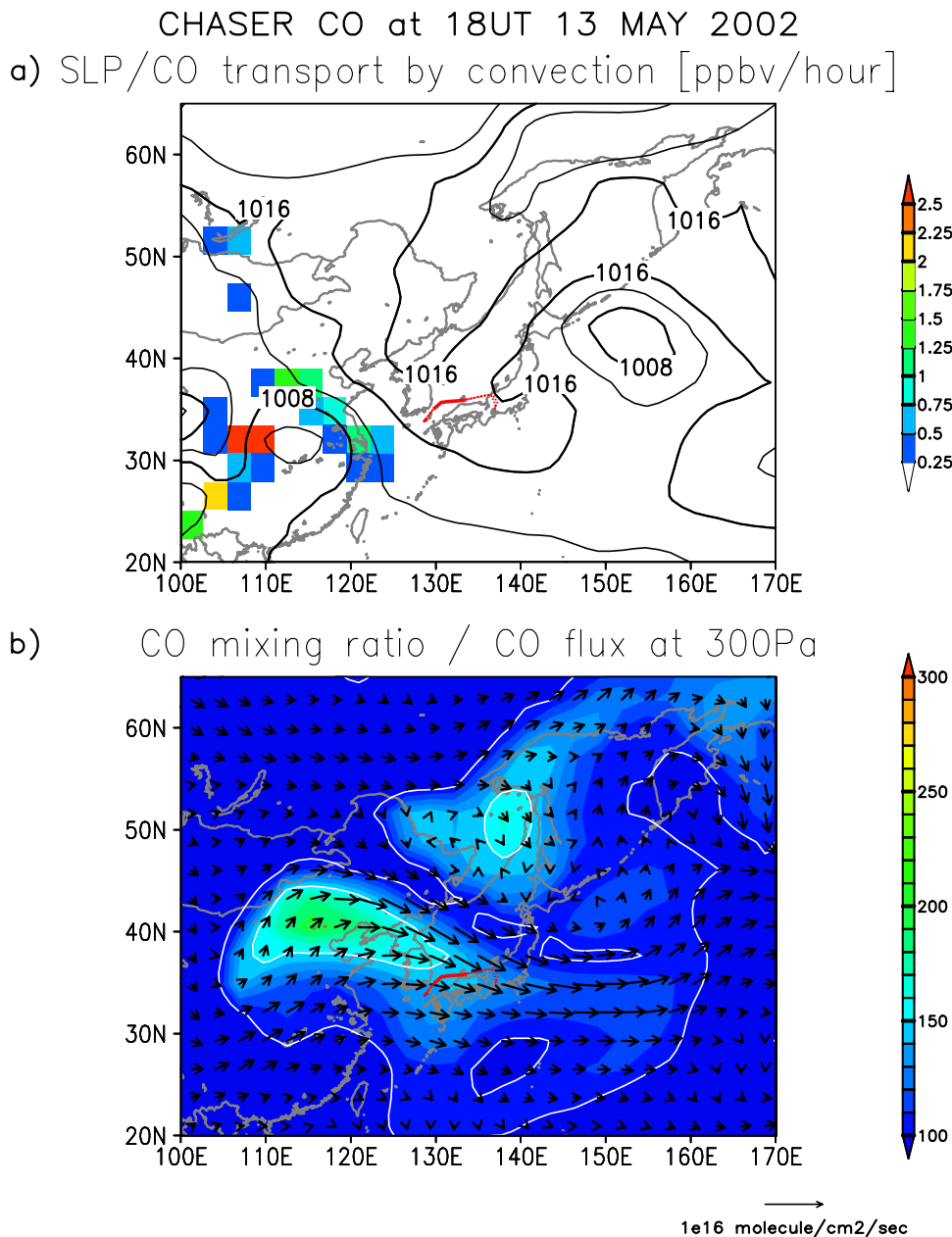
Figure 18. (a) Sea level pressure (contours, units of hPa), and CO tendency by convective transport at 300 hPa at 18:00 UTC on 13 May 2002 (color tones, units of ppbv/hour). (b) CO mixing ratio and horizontal CO flux at 300 hPa at 18:00 UTC on 13 May 2002. The contour interval is 50 ppbv. The unit length is shown below the figure. Red lines denote the track of flight 10 of PEACE−B on 14 May 2002, and the leg from 6:48 UTC to 7:22 UTC is shown with the bold line.

the model shows similar UT CO enhancement. The correlation coefficient between the observed and calculated ΔCO for this flight is 0.56 in the FT. The CO concentration is observed to increase from about 120 ppbv outside the plume to around 300 ppbv in the plume. There is a similar increase in the modeled CO profile, although the modeled CO increase is smaller, from 80 to 145 ppbv, and the increase is restricted to 300–350 hPa. Tagged CO tracers suggest that emissions from southern China are responsible for this enhanced UT plume. Emissions from southern China comprise 18–21% of the total CO mixing ratio in the plume.

Emissions from northern China contribute 8–10% of the total CO in the plume.

[30] Figure 18 shows the sea level pressure, CO mixing ratio tendency forced by convective transport at 300 hPa, CO fluxes at 300 hPa, and modeled CO mixing ratio at 300 hPa calculated by CHASER. Figure 18 also show the track of flight 10 during PEACE−B on 14 May 2002. A mid−latitude cyclone was over central China on 13 May. Warm, moist southerly winds in the lower troposphere intensified ahead of this surface cyclone over southern China, converging into a front extending between 20°N,
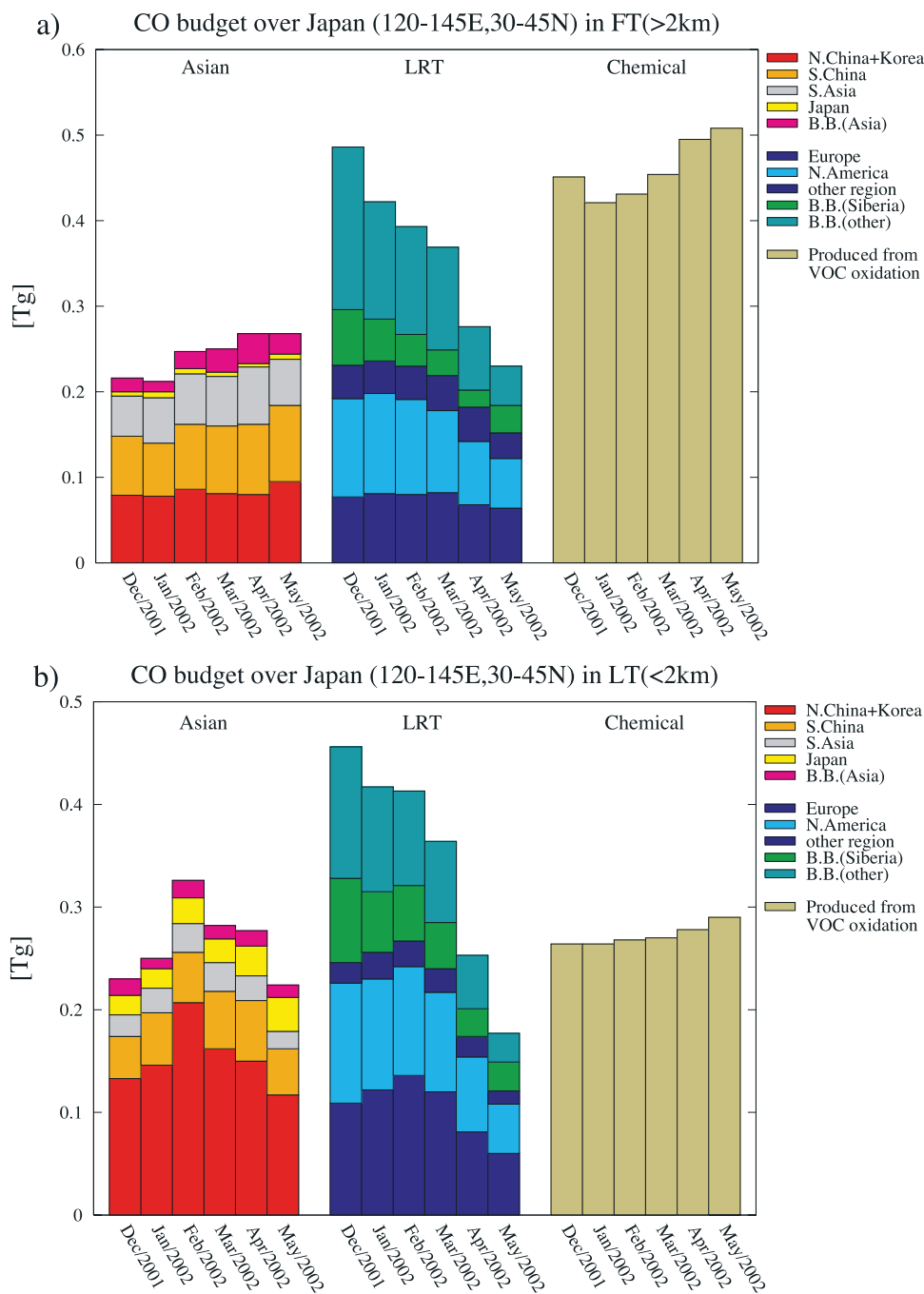
Figure 19. The calculated monthly mean net CO budget over Japan (120°-145°E, 30°-45°N). The units are TgCO. (a) The CO budget for the free troposphere (above 2 km). (b) The CO budget for the lower troposphere (below 2 km).

100°E and 30°N, 115°E. Deep convective clouds, with tops above 10 km around 30°N, 105°−120°E, are found in an infrared (IR) image obtained by the Geostationary Meteorological Satellite (GMS)−5 (see Figure 6d of *Oshima et al.* [2004]). CO over southern Asia in the UT was transported by southerly LT winds over southern China, and trapped by the cumulus convection in that area. The model reproduces similar convective activity around the cyclone and models the CO changes influenced by convective transport, as shown in Figure 18a. Convective transport changes the CO concentration at an estimated rate of 0.5−3.0 ppbv/hour at

300 hPa over central China. The mass change of CO in the free troposphere caused by the uplift of cumulus convection was calculated by using cloud base mass flux and detraining mass flux in the model. The mass change of CO by the downdraft is also considered, but the effect is small compared to the uplift over central China. The convective processes associated with this cyclone began on 12 May 2002. Consequently, convection transported about 0.3 TgCO on 12−13 May 2002, and the maximum height of the CO concentration increase caused by convective transport is between 300−400 hPa. A high CO region with the
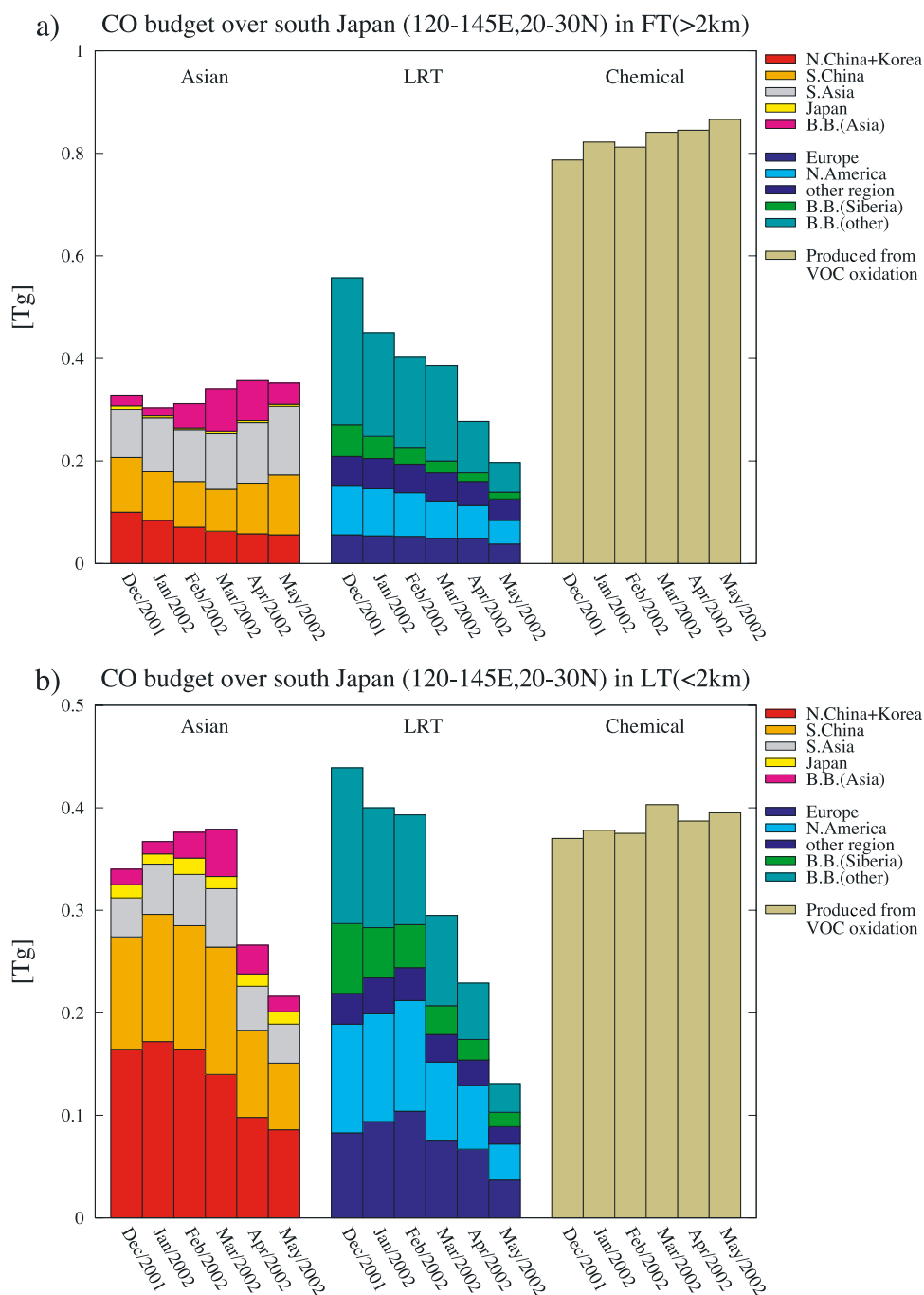
Figure 20. As in Figure 19, but for the area south of Japan (120°–145°E, 20°–30°N).

value of 150 ppbv or higher can be seen over northern China and Korea in Figure 18b. The modeled CO increase by convective transport was not bee seen at 450 hPa over central China. The model tends to underestimate the detrainment of middle convection, and it is the probable reason why the model was not able to reproduce the CO increase at 450 hPa during flight 10 of PEACE–B. Five–day back trajectories for air parcels in which the highest CO mixing ratios were observed during flight 10 of PEACE-B indicate that these high–CO air parcels were located over central China (around 30°N, 115°E) 24 hours prior to the measurement (see Figures 5a and 5b of *Oshima et al.* [2004]). The CO over

central China increased from 0.98 Tg on 11 May to 1.28 Tg on 13 May between 300 and 400 hPa. The plume over central China was transported from the surface by the cumulus convection on 12–13 May. It was subsequently advected by westerly winds and moved over central Japan on 13–14 May.

4.7. Net CO Budget During the PEACE Campaign

[31] Figure 19 shows the CO budget over Japan (120°–145°E, 30°–45°N). The CO budget is categorized by origin, and includes three source types: the Asian CO tracers, the LRT CO tracers, and the chemically produced CO tracer). In

the free troposphere, the LRT CO tracers are especially high in winter. The total CO budget over Japan in the free troposphere is about 1.15 TgCO in January. About 36% of the CO originates from surface emissions outside Asia. *Liang et al.* [2004] examined the influence of Asian emissions on CO levels throughout the North Pacific with the GEOS–CHEM global three-dimensional model, and found that Asian influence was estimated to be 41% of total CO in the western Pacific troposphere. The model estimated that about 30% of the total CO over Japan in LT was influenced by the Asian CO in March. The contribution of the LRT CO tracers to the total CO in late spring is relatively small because of the enhanced chemical activity and weakened zonal jet. LRT CO comprises less than 20% of the total CO budget in May. The CO contribution from Asia to CO in the FT over Japan increase from winter to spring as cumulus convection increases in late spring. In the boundary layer, CO originating over northern China shows value exceeding 0.1 TgCO. The fraction of the north Chinese CO to the total CO budget in the boundary layer reaches a maximum of 21% during this period. The mean wind direction during PEACE–A was northwesterly in the boundary layer (see also Figure 2 of *Kondo et al.* [2004]) because of the dominant Siberian High.

[32] Figure 20 shows the CO budget over southern Japan ($120°$–$145°E$, $20°$–$30°N$). The tropospheric flow in this region was westerly during PEACE–A and PEACE–B. The contributions by the LRT CO to the total CO are relatively small compared to over Japan (Figure 19). The flow in the boundary layer was northwesterly during PEACE–A, and easterly or southerly during PEACE–B, when winds transported maritime air into the region. The Asian CO in the budget decreased in April and May in the boundary layer, as the wind direction changed.

5. Summary and Conclusions

[33] Global chemical weather forecasts made with CHASER can be useful in planning flights targeting different types of synoptic scale phenomena, such as near–surface outflow from nearby polluted regions, or intercontinental plumes of pollutions in the middle and upper troposphere. The chemical forecast produced by the model was able to reproduce the CO values observed during the PEACE–A and PEACE–B campaign. The values were within 10–20% of the observed mixing ratios at three ground–based observational sites in the major sampling region of PEACE, and within 20–30% of the airborne observed mean mixing ratios during PEACE. The ability to reproduce spatial and temporal variability is critical for flight planning. Although the model underestimates the background CO level by 20–40 ppbv compared with observations in late spring, the model can still reproduce the transport of polluted air masses in the free troposphere. The model estimated the convective transport of CO. The results suggest that about a half of the emissions over China are affected by the cumulus convection over China in late spring. The meridional and seasonal variation in the LRT CO, Asian CO, and CO produced by the oxidation of CH_4 and NMHCs were all evaluated using tagged CO tracers. LRT CO comprised about 36% of the total CO budget in winter, and about 20% in spring, in the free troposphere

over Japan. In late spring, the influence of Asian CO over southern Japan decreased compared to that in winter as the wind direction shifted from northwesterly to easterly or southerly.

[34] One particular factor that is closely linked to the quality of chemical weather forecasts is the data quality of surface boundary. For example, diurnal, daily, and weekly cycles in anthropogenic surface emissions, and stochastic natural emissions, such as forest fires, must be considered. An approach to improve the evaluation of these surface emissions is to assimilate satellite observations [e.g., *Chin et al.*, 2003]. The stratospheric O_3 fluxes could be improved if the stratospheric chemical process in *Takigawa et al.* [2002] were imported into the model. Since higher–resolution models consistently provide better forecasts of local convection or the fine–scale transport structure, it is important to increase the horizontal and vertical resolution. Nested models could focus on a particular region with simulation that interacts with the global environment [e.g., *Wang et al.*, 2004; *Peters et al.*, 2004]. Important refinement are also needed in the chemical and physical algorithms for aerosols and soluble gases, and for the interaction between aerosols and clouds. *Takemura et al.* [2000] coupled the CCSR/NIES AGCM with aerosol processes, and key features of the aerosol processes in that model will be considered in a future version of our model. There are several chemical weather forecasting systems for global and regional scale forecasting. Comparison of these models will be useful for evaluating the chemical processes used by each model.

References

Arakawa, A., and W. Schubert (1974), Interactions of cumulus cloud ensemble with the large–scale environment. Part I, *J. Atmos. Sci.*, *31*, 671–701.

Arino, O., J.-M. Rosaz, and J.-M. Melinotte (1999), World Fire Atlas with AVHRR and ATSR, paper presented at IUFRO Conference on Remote Sensing and Forest Monitoring.

Bertschi, I., D. Jaffe, L. Jaeglé, H. Price, and J. Dennison (2004), PHOBEA/ITCT 2002 airborne observations of transpacific transport of ozone, CO, volatile organic compounds, and aerosols to the northeast Pacific: Impacts of Asian anthropogenic and Siberian boreal fire emissions, *J. Geophys. Res.*, *109*, D23S12, doi:10.1029/2003JD004328.

Chin, M., et al. (2003), A global aerosol model forecast for ACE–Asia field experiment, *J. Geophys. Res.*, *108*(D23), 8654, doi:10.1029/2003JD003642.

Colella, P., and P. Woodward (1984), The Piecewise Parabolic Method PPM for Gas–Dynamic Simulations, *J. Comput. Phys.*, *54*, 174–201.

Cooper, O., et al. (2001), Trace gas signatures of the airstreams within North Atlantic cyclones: Case studies from the NARE '97 aircraft intensive, *J. Geophys. Res.*, *106*, 5437–5456.

Cox, R., et al. (2005), Summary of evaluated kinetic and photochemical data for atmospheric chemistry. (Available at http://www.iupac-kinetic.ch.cam.ac.uk/)

Emori, S., T. Nozawa, A. Numaguti, and I. Uno (2001), Importance of cumulus parameterization for precipitation simulation over East Asia in June, *J. Meteorol. Soc. Jpn.*, *79*, 939–947.

Flatøy, F., O. Hov, and H. Schlager (2000), Chemical forecasts used for measurement flight planning during POLINAT 2, *Geophys. Res. Lett.*, *27*, 951–954.

Holslag, A., and B. Boville (1993), Local versus nonlocal boundary–layer diffusion in a global climate model, *J. Clim.*, 6, 1825–1842.

Kiley, C., et al. (2003), An intercomparison and evaluation of aircraft–derived and simulated CO from seven chemical transport models during the TRACE–P experiment, *J. Geophys. Res.*, 108(D21), 8819, doi:10.1029/2002JD003089.

Kondo, Y., et al. (2004), Photochemistry of ozone over the western Pacific from winter to spring, *J. Geophys. Res.*, 109, D23S02, doi:10.1029/2004JD004871.

Lawrence, M., et al. (2003), Global chemical weather forecasts for field campaign planning: predictions and observations of large–scale features during MINOS, CONTRACE, and INDOEX, *Atmos. Chem. Phys.*, 3, 267–289.

Lee, A., G. Carver, M. Chipperfield, and J. Pyle (1997), Three–dimensional chemical forecasting: A methodology, *J. Geophys. Res.*, 102, 3905–3919.

Liang, Q., L. Jaeglé, D. A. Jaffe, P. Weiss-Penzias, A. Heckman, and J. Snow (2004), Long–range transport of Asian pollution of the northeast Pacific: Seasonal variations and transport pathways of carbon monoxide, *J. Geophys. Res.*, 109, D23S07, doi:10.1029/2003JD004402.

Lin, S.-J., and R. Rood (1996), Multidimensional flux–form semi–Lagrangian transport schemes, *Mon. Weather Rev.*, 124, 2046–2070.

Liu, H., D. Jacob, I. Bey, R. Yantosca, and B. Duncan (2003), Transport pathway for Asian pollution outflow over the Pacific: Interannual and seasonal variations, *J. Geophys. Res.*, 108(D20), 8786, doi:10.1029/2002JD003102.

McCabe, D., T. Gierczak, R. Talukdar, and A. Ravishankara (2001), Kinetics of the reaction plus CO undeer atmospheric conditions, *Geophys. Res. Lett.*, 28, 3135–3138.

Mellor, G. L., and T. Yamada (1974), A hierarchy of turbulence closure models for planetary boundary layers, *J. Atmos. Sci.*, 31, 1791–1806.

Nakajima, T., M. Tsukamoto, Y. Tsusima, and A. Numaguti (1995), Modeling of the radiative process in a AGCM, in *Reports of a New Program for Creative Basic Research Studies, Studies of Global Environment Change to Asia and Pacific Regions*, Rep. I-3, pp. 104–123, CCSR, Tokyo.

Numaguti, A. (1993), Dynamics and energy balance of the Hadley circulation and the tropical precipitation zones: Significance of the distribution of evaporation, *J. Atmos. Sci.*, 50, 1874–1887.

Numaguti, A., M. Takahashi, T. Nakajima, and A. Sumi (1995), Development of an atmospheric general circulation model, in *Reports of a New Program for Creative Basic Research Studies, Studies of Global Environment Change to Asia and Pacific Regions*, Rep. I-3, pp. 1–27, CCSR, Tokyo.

Numaguti, A., M. Takahashi, T. Nakajima, and A. Sumi (1997), Development of CCSR/NIES Atmospheric General Circulation Model, *CGER's Supercomput. Monogr. Rep.*, vol. 3, pp. 1–48, CGER, Tsukuba, Ibaraki.

Olivier, J. G. J., A. F. Bouwman, C. W. M. V. der Maas, J. J. M. Berdowski, C. Veldt, J. P. J. Bloos, A. J. H. Visschedijk, P. Y. J. Zandveld, and J. L. Haverlag (1996), Description of EDGAR Version 2.0. A set of global emission inventories of greenhouse gases and ozone-depleting substances for all anthropogenic and most natural sources on a per country basis and on $1° \times 1°$ grid, *RIVM/TNO Rep. 711060 002*, p. 1006, RIVM, Bilthoven.

Oshima, N., et al. (2004), Asian chemical outflow to the Pacific in late spring observed during the PEACE–B aircraft mission, *J. Geophys. Res.*, 109, D23S05, doi:10.1029/2004JD004976.

Pan, D.-M., and D. Randall (1998), A cumulus parameterization with a prognostic closure, *Q. J. R. Meteorol. Soc.*, 124, 949–981.

Parrish, D., Y. Kondo, O. Cooper, C. Brock, D. Jaffe, M. Trainer, T. Ogawa, G. Hübleer, and F. Fehsenfeld (2004), Intercontinental Transport and Chemical Transformation 2002 (ITCT 2K2) and Pacific Exploration of Asian Continental Emission (PEACE) experiments: An overview of the 2002 winter and spring intensives, *J. Geophys. Res.*, 109, D23S01, doi:10.1029/2004JD004980.

Peters, W., et al. (2004), Toward regional–scale modeling using the two–way nested global model TM5: Characterization of transport using sf$_6$, *J. Geophys. Res.*, 109, D19314, doi:10.1029/2004JD005020.

Streets, D., et al. (2003), An inventory of gaseous and primary aerosol in Asia in the year 2000, *J. Geophys. Res.*, 108(D21), 8809, doi:10.1029/2002JD003093.

Sudo, K., M. T. J. ichi Kurokawa, and H. Akimoto (2002a), CHASER: A global chemical model of the troposphere 1. Model description, *J. Geophys. Res.*, 107(D21), 4339, doi:10.1029/2001JD001113.

Sudo, K., M. Takahashi, and H. Akimoto (2002b), CHASER: A global chemical model of the troposphere 2. Model results and evaluation, *J. Geophys. Res.*, 107(D21), 4586, doi:10.1029/2001JD001114.

Sudo, K., M. Takahashi, and H. Akimoto (2003), Future changes in stratosphere–troposphere exchange and their impacts on future tropospheric ozone simulations, *Geophys. Res. Lett.*, 30(24), 2256, doi:10.1029/2003GL018526.

Takemura, T., H. Okamoto, Y. Maruyama, A. Numaguti, A. Higurashi, and T. Nakajima (2000), Global three-dimensional simulation of aerosol optical thickness distribution of various origins, *J. Geophys. Res.*, 105, 17,853–17,873.

Takigawa, M., M. Takahashi, and H. Akiyoshi (2002), Simulation of stratospheric sulfuric acid aerosol using a Center for Climate System Research/National Institute for Environmental Studies atmospheric GCM with coupled chemistry: Part I, nonvolcanic simulation, *J. Geophys. Res.*, 107(D22), 4610, doi:10.1029/2001JD001007.

Treut, H. L., and Z.-X. Li (1991), Sensitivity of an atmospheric general circulation model to prescribed SST changes: feedback effects associated with the simulation of cloud optical properties, *Clim. Dyn.*, 5, 175–187.

Uno, I., et al. (2003), Regional chemical weather forecasting system CFORS: Model descriptions and analysis of surface observations at Japanese island stations during the ACE–Asia experiment, *J. Geophys. Res.*, 108(D23), 8668, doi:10.1029/2002JD002845.

von Kuhlmann, R., M. Lawrence, U. Pöschl, and P. Crutzen (2004), Sensitivities in global scale modeling of isoprene, *Atmos. Chem. Phys.*, 4, 1–17.

Wang, Y., M. McElroy, D. Jacob, and R. Yantosca (2004), A nested grid formulation for chemical transport over Asia: Application to CO, *J. Geophys. Res.*, 109, D22307, doi:10.1029/2004JD005237.

Yurganov, L., et al. (2005), Increased Northern Hemispheric carbon monoxide burden in the troposphere in 2002 and 2003 detected from the ground and from space, *Atmos. Chem. Phys.*, 5, 563–573.

————————————

H. Akimoto, K. Sudo, and M. Takigawa, Frontier Research Center for Global Change, Japan Marine Science and Technology, 3173-25 Showamachi, Kanazawa-ku, Yokohama, Kanagawa 236-0001, Japan. (akimoto@jamstec.go.jp; kengo@jamstec.go.jp; takigawa@jamstec.go.jp)

K. Kita, Department of Environmental Science, Graduate School of Science, Ibaraki University, 2–1–1 Bunkyo, Mito, Ibaraki 310–8512, Japan. (kita@env.sci.ibaraki.ac.jp)

Y. Kondo and N. Takegawa, Research Center for Advanced Science and Technology, University of Tokyo, 4-6-1, Komaba, Meguro-Ku, Tokyo 153–8904, Japan. (kondo@atmos.rcast.u-tokyo.ac.jp; takegawa@atmos.rcast.u-tokyo.ac.jp)

M. Takahashi, Center for Climate System Research, University of Tokyo, 5–1–5, Kashiwanoha, Kashiwa–shi, Chiba 277–8568, Japan. (masaaki@ccsr.u-tokyo.ac.jp)